telecom

MDPI

Article

Preliminary Visibility Studies with 1-Min Integration Time for the Planning and Dimensioning of Free-Space Optical Systems in Colombia

Juan C. Navarro-Ramos [1], Duvan Darío Quintero-Cardozo [1], María E. Rojas-Méndez [2], Nelson A. Pérez-García [2,*], Ángel D. Pinto-Mangones [3], Juan M. Torres-Tovio [3], Octavio A. Torres-Medina [2] and Yair Rivera Julio [4]

[1] Specialization in Information Technologies, Universidad del Sinú, Monteria 230001, Colombia; juannavarro@unisinu.edu.co (J.C.N.-R.); duvandquintero@unisinu.edu.co (D.D.Q.-C.)
[2] Postgraduate Program in Telecommunications, Universidad de Los Andes, Merida 5101, Venezuela; maru0544@gmail.com (M.E.R.-M.); octa022@gmail.com (O.A.T.-M.)
[3] Systems Engineering Program, Universidad del Sinú, Monteria 230001, Colombia; angelpinto@unisinu.edu.co (Á.D.P.-M.); juantorres@unisinu.edu.co (J.M.T.-T.)
[4] Department of Computer Science, Corporación Universitaria Americana, Barranquilla 080001, Colombia; yrivera@americana.edu.co
* Correspondence: perezn@ula.ve

Abstract

This work presents, for the first time, visibility measurements carried out in five locations in Colombia (Yopal, San Andrés, Montería, Puerto Carreño, and Villavicencio) during their respective months of lowest visibility, using Vaisala FD70 forward-scatter sensors with a 1-min integration time. The cumulative distributions (CDs) of visibility obtained are fundamental for estimating fog attenuation in free-space optical (FSO) communication systems operating at optical frequencies. Additionally, the performance of visibility prediction models reported in the literature (the Sousa, Queluz, and Rodrigues model, hereafter referred to as the SQR model, and the Pinto I and Pinto II models) is evaluated within the Colombian climatic context. It was observed that the Pinto I and Pinto II models exhibited the best overall performance among the existing models, with a root mean square error (RMSE) value close to 11.46 km for the set of locations, while the locality of San Andrés presented the most adverse conditions, with visibilities below 50 m for 0.01% of the time during the critical month of November. A link-budget analysis shows that the use of visibility prediction models can lead to severe underdimensioning or overdimensioning of FSO links, highlighting the need for locally measured visibility data.

Keywords: visibility; FSO systems; 1-min integration time; visibility prediction models; critical month; fog attenuation; link budget

Check for updates

Academic Editor: Hector E. Nistazakis

Received: 11 May 2026
Revised: 16 July 2026
Accepted: 24 July 2026
Published: 5 August 2026

Copyright: © 2026 by the authors. Licensee MDPI, Basel, Switzerland. This article is an open access article distributed under the terms and conditions of the Creative Commons Attribution (CC BY) license.

1. Introduction

Free-space optical communications (FSO, Free-Space Optics) have emerged as a complementary technology to optical fiber networks and conventional radiofrequency (RF) links [1,2]. In a context where fifth- and sixth-generation (5G/6G) networks demand bandwidths on the order of Gbps, with extremely low latencies and unprecedented connection densities, FSO systems offer major advantages: rapid deployment without the need for costly civil works, operation in unlicensed spectrum (which eliminates licensing costs), immunity to electromagnetic interference, and superior physical-layer security due to the narrowness of the laser beam [3,4].

However, the massive deployment of FSO systems faces a critical obstacle: the propagation channel is the Earth's atmosphere. Unlike RF signals above 10 GHz, which are mainly affected by rainfall, optical signals that typically operate at wavelengths between 780 nm (384.62 THz) and 1550 nm (193.55 THz) are extremely sensitive to the presence of aerosols and suspended hydrometeors [5]. Among these phenomena, fog and mist represent the main limiting factor for the availability of FSO systems, since suspended water droplets, whose size is comparable to the laser wavelength, produce a Mie scattering phenomenon that can generate specific attenuations greater than 300 dB/km under dense fog conditions [6,7].

Meteorological visibility, defined by the World Meteorological Organization (WMO) as the maximum distance at which a black object of appropriate dimensions can be recognized against the horizon, is the fundamental parameter for quantifying fog attenuation [8]. The relationship between specific attenuation, γ [dB/km], and visibility, V [km] has been widely studied, giving rise to models such as Kruse [9] and Kim–McArthur–Korevaar [10], which constitute the basis of the recommendations of the International Telecommunication Union (ITU) for the design of terrestrial FSO links [11].

Nevertheless, for the rigorous planning and dimensioning of FSO systems, it is not sufficient to know a point visibility value. It is necessary to know the cumulative distribution (CD) of visibility, that is, the visibility value that is not exceeded during a given percentage of time, $p(\%)$, over an average annual period or, preferably, during the worst month (understood as the month in which, on average, visibility is lowest [12,13]), or at least during the critical months identified from historical data (a more conservative situation, which was considered in this work because measurements over at least an annual period were not available). This requirement is analogous to that established by the ITU for the planning and dimensioning of radiofrequency links operating above 10 GHz, where it is also required that the precipitation distribution has been measured or estimated with a 1-min integration time [14]. In the case of FSO links, high temporal resolution (1-min) is indispensable to capture the dynamics of fog formation and dissipation, making it possible to predict how many minutes per year the link will be out of service.

Given the limited availability of local visibility statistics with 1-min resolution in many regions of the world (most visibility measurements are reported at broad time intervals, for example, in hours [15]), as is the case of Colombia, this situation makes it necessary to resort to models reported in the literature that allow such distributions to be estimated from more easily accessible meteorological information (for example, the average number of fog days per year and the average duration of fog events), with the model proposed by Sousa, Queluz, and Rodrigues (called the SQR model) [15] and the models developed by Pinto-Mangones et al. (referred to in this study as the Pinto I and Pinto II models) [16], being, to date, the only ones that allow visibility to be estimated as a function of the percentage of time. However, the aforementioned models were derived from fitting visibility data in temperate climate regions (for example, Portugal) or from global databases that do not faithfully reflect the tropical climatic conditions of Colombia.

Accordingly, preliminary studies carried out for this article in Colombian localities such as Montería and San Andrés have shown that the above existing models drastically underestimate or overestimate visibility, introducing considerable uncertainty into the prediction of FSO link performance. This disparity can lead to overdimensioning (which entails unnecessary capital expenditure) or underdimensioning (which leads to quality-of-service and availability problems) [17].

In view of the aforementioned problem, this article presents the following original contributions: (i) presentation of the first complementary cumulative distributions of visibility with a 1-min integration time for five representative localities in Colombia (Yopal,

San Andrés, Montería, Puerto Carreño, and Villavicencio), obtained during their respective months of lowest visibility; (ii) quantitative evaluation of the performance of existing visibility prediction models (SQR, Pinto I, and Pinto II) in the Colombian climatic context, using the RMSE metric; and (iii) identification of the most critical localities and conditions for the deployment of FSO systems in Colombia, providing criteria for the planning of optical backhaul networks in the country.

Finally, the rest of the article is organized as follows. Section 2 describes the visibility measurement network used, including the selected localities, the identified critical months, the measurement equipment (Vaisala FD70), and the data processing procedure. Section 3 presents the experimental results, including the cumulative visibility distributions. Section 4 implements and evaluates the performance of the existing prediction models (SQR, Pinto I, and Pinto II) through qualitative and quantitative analysis (RMSE value). Section 5 discusses the implications of the results for the planning of FSO systems in Colombia. Finally, Section 6 presents the conclusions of the research and recommendations for future work.

2. Visibility Measurement Network in Colombia

2.1. Selected Localities and Critical Months

For this research, it was possible to use measurements carried out in five Colombian localities representative of different climatic and geographic conditions: Yopal (Casanare, transition region between the Andes and the Orinoquía), San Andrés (island in the Caribbean Sea, tropical coastal zone), Montería (Córdoba, northern Colombia with coastal influence), Puerto Carreño (Vichada, Orinoquía region), and Villavicencio (Meta, Llanos foothills). Figure 1 shows the geographic distribution of the five aforementioned localities, while Table 1 presents the geographic coordinates of each airport where the measurements were carried out.



Figure 1. Geographic distribution of the localities considered in this research.

Table 1. Geographic coordinates of the localities studied.

Airport	Locality	Latitude (+N)	Longitude (+E)
El Alcaraván	Yopal	5.324	−72.382
Gustavo Rojas Pinilla	San Andrés	12.585	−81.708
Los Garzones	Montería	8.825	−75.824
Germán Olano	Puerto Carreño	6.184	−67.491
Vanguardia	Villavicencio	4.165	−73.618

Given the difficulty of having measurements carried out for at least an average annual period, the measurement campaigns considered in this research focused on the months of the year in which the lowest visibility is historically present (critical month) for each locality, identified from historical records of the Civil Aeronautics of Colombia, under the understanding that, by planning and dimensioning an FSO system so that it operates adequately during the month or months of lowest visibility, the operation of the system during the rest of the average annual period will be guaranteed. The aforementioned months are as follows:

- Yopal: March and April 2025.
- San Andrés: October and November 2024.
- Montería: October 2024 and April 2025.
- Puerto Carreño: April 2025.
- Villavicencio: March and April 2025.

The identification of these critical months was carried out internally by the Civil Aeronautics of Colombia based on their own historical visibility records; the specific historical period and internal methodology underlying this institutional identification were not disclosed to the authors. The Civil Aeronautics of Colombia provided the authors, under a confidentiality agreement, only the 1-min visibility time series corresponding to the critical months already identified for each locality, listed above.

It should be noted that this critical-month approach, while conservative for planning purposes, does not capture inter-annual variability in fog occurrence or the complete seasonal cycle. This constitutes a limitation of the present study, addressed further in Section 6.

2.2. Measurement Equipment

For visibility measurement, the Civil Aeronautics of Colombia used a Vaisala FD70 forward-scatter sensor whose operating principle is illustrated in Figure 2a, while Figure 2b shows a reference image of said sensor [18].

The Vaisala FD70 sensor employs a forward-scatter measurement principle with fixed look-down geometry [18,19]. The transmitter (TX) projects a beam of infrared light obliquely toward the Earth's surface. When the beam encounters suspended particles (such as fog droplets), these form a sample volume that scatters the light in all directions, as observed in Figure 2a. The transmitter and the main receiver (RX1) are arranged so that their optical axes form a scattering angle of 42°, considered optimal for visibility measurement [18]. The main receiver measures the intensity of the light scattered at that angle, which is directly correlated with the atmospheric extinction coefficient, from which the Meteorological Optical Range (MOR), that is, meteorological visibility, is calculated.

Additionally, as also shown in Figure 2a, the sensor incorporates a secondary receiver (RX2) whose optical axis forms a 90° angle with respect to the emitter axis, being more sensitive to larger particles (raindrops, snowflakes), which allows the type of precipitation to be identified [18]. This dual configuration (receivers at 42° and 90°) makes it possible for

the sensor not only to quantify visibility but also to discriminate between fog, rain, and other forms of precipitation.

For its part, the look-down geometry (beam projected toward the ground), together with the heating system in the optical windows, that is, the protected but exposed surfaces through which the sensor emits and receives light to measure visibility, minimizes interference due to the accumulation of dirt, snow, or ice on the optical surfaces, guaranteeing reliable measurements under adverse climatic conditions [18].

Figure 2b shows a photograph of the Vaisala FD70 sensor in its typical installation configuration. The equipment complies with the requirements of the International Civil Aviation Organization (ICAO), the Federal Aviation Administration (FAA), and the World Meteorological Organization (WMO) [18], and it is widely used in airport and meteorological applications.

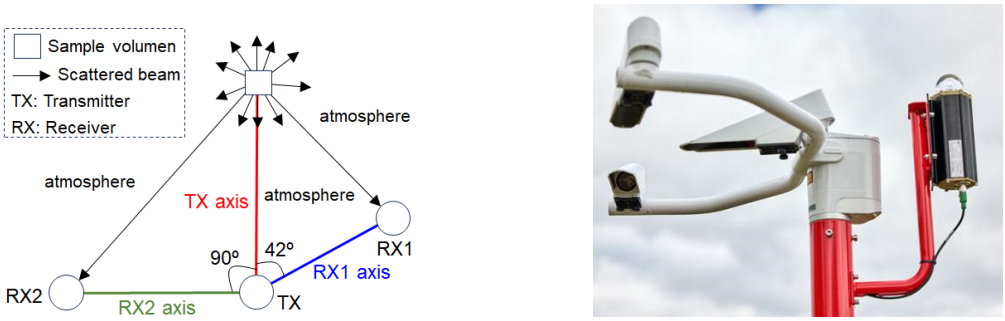


Figure 2. Vaisala FD70 visibility sensor: (**a**) Schematic diagram of the forward-scatter measurement principle, including the emitter (TX), the receivers (RX1 and RX2), the scattering angles of 42° and 90°, and the sample volume; (**b**) Vaisala FD70 sensor.

It should be noted that, at the airports of San Andrés and Montería, measurements from more than one sensor were initially available. In both scenarios, it was decided to select the time series corresponding to the worst case for the purposes of planning and dimensioning FSO systems, specifically, the time series that yielded the cumulative distributions with lower visibility values.

2.3. Data Processing

The visibility time series with a 1-min integration time (although the measurement cycle of the equipment is 5 s, the average value was stored every 1-min) were subjected to a filtering process to eliminate anomalous values, typically associated with periods of equipment maintenance, calibration, or transient failures. The quality control procedure included the elimination of records with null values without meteorological justification and abrupt visibility changes without an associated meteorological cause [8,20].

After the filtering process, the effective data availability for each locality was high: 95% for San Andrés; 96% for Yopal, Montería, and Villavicencio; and 97% for Puerto Carreño.

From the filtered time series, the cumulative distributions of visibility, $P(V)$, were constructed. These distributions indicate the visibility value (in km) that is not exceeded during a percentage of time $p(\%)$ of the measurement period, according to the following:

$$P(V) = P(V \leq v) = F_V(v) = \frac{\text{number of records with } V \leq v}{\text{total number of records}} \times 100\% \quad (1)$$

where V is the random variable, specifically, the measured visibility (which can take different values), and v refers to the specific value or threshold (for example, v = 3 km).

Figure 3 summarizes the complete methodological workflow followed in this study, from locality selection to the final link-budget/dimensioning impact analysis.

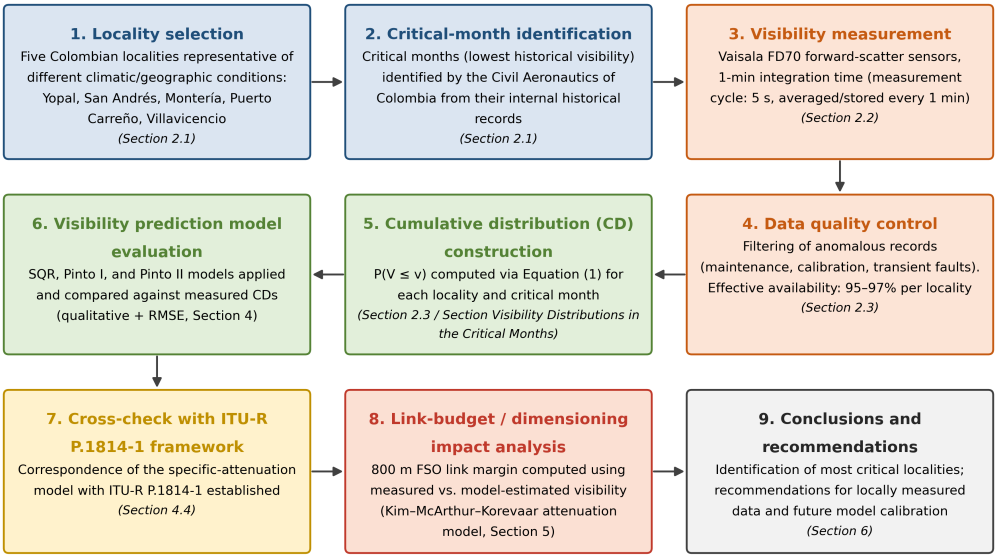


Figure 3. Methodological workflow followed in this study.

3. Measurement Results

Visibility Distributions in the Critical Months

Figure 4 presents the cumulative distributions of visibility with a 1-min integration time for the five localities studied, corresponding to their respective months of lowest visibility.

In Figure 4, the following can be observed:

- **Yopal (Figure 4a)**: The behavior of visibility is irregular and seasonal. For $p = 0.01\%$, March records 0.59 km and April 0.16 km; for $p = 0.1\%$, 1.06 km versus 0.57 km, respectively. However, from $p = 8\%$ onward, the curves converge and present similar visibility values up to $p = 10\%$, the upper limit of the percentage-of-time range considered in this study. Therefore, it could be inferred that, within this range, seasonal differences in Yopal are concentrated in the lowest percentages of time ($p \leq 8\%$), while for $8\% < p \leq 10\%$, visibilities in March and April are practically the same.
- **San Andrés (Figure 4b)**: This island locality presents characteristics of a coastal zone with extremely adverse conditions. For example, in November, for $p = 0.01\%$, visibility drops to 48 m and for $p = 1\%$ reaches only 287 m. In October, the situation is slightly better, with visibilities of 147 m and 666 m for the same percentages, respectively. These results indicate that San Andrés presents extreme conditions for FSO links, with dense fog reducing visibility to less than 200 m for a small percentage of time.
- **Montería (Figure 4c)**: At $p = 0.01\%$, October presents a visibility of 0.29 km compared with 0.39 km in April. For $p = 0.1\%$, the values are 0.41 km in October and 1.09 km in April. Nevertheless, the curves cross near $p = 3\%$, reaching 10.54 km in October and 9.75 km in April at $p = 4\%$. This suggests that April is better only in the most extreme percentages (very low visibility), while October dominates during the rest of the time, revealing a distribution more extended toward low values in October, although for $3\% < p \leq 10\%$, within the range considered in this study, visibility in October is systematically higher than in April.
- **Puerto Carreño (Figure 4d)**: This locality shows moderately high visibilities, with 0.631 km for $p = 0.01\%$ and 7.32 km for $p = 1\%$. The distribution shows a more gradual behavior than in other localities, i.e., visibility does not present sudden jumps between nearby percentiles.

- **Villavicencio (Figure 4e)**: In April, visibilities are systematically higher than in March across the entire percentage range (the curves do not intersect). For example, for $p = 0.01\%$, March records 0.62 km and April 2.60 km; for $p = 0.1\%$, 0.79 km versus 4.41 km, respectively; for $p = 1\%$, 9.96 km versus 14.95 km; and for $p = 10\%$, 39.62 km versus 53.11 km. This indicates that April offers better visibility conditions than March both in extreme episodes and during most of the time.

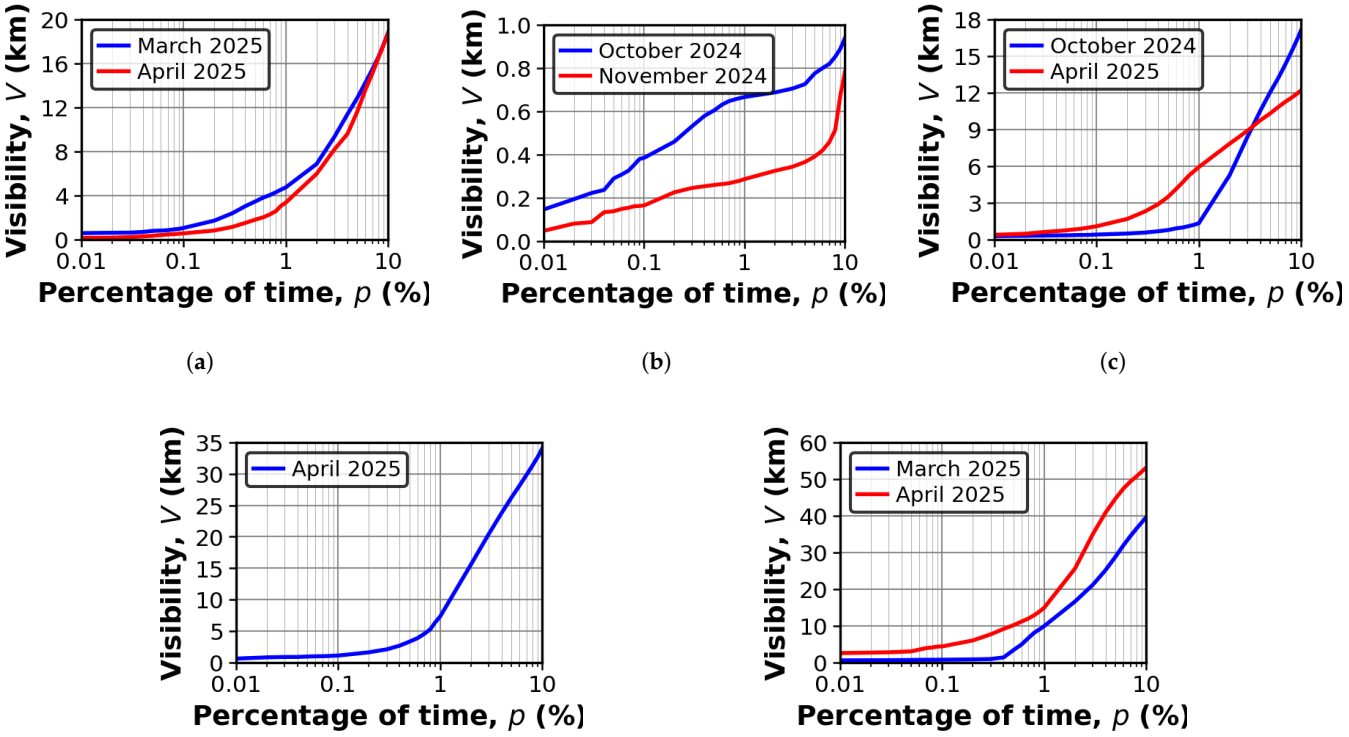


Figure 4. Cumulative visibility distributions with 1-min integration time, measured in the critical months (lowest visibility): (**a**) Yopal; (**b**) San Andrés; (**c**) Montería; (**d**) Puerto Carreño; (**e**) Villavicencio.

4. Evaluation of Visibility Prediction Models for Use in FSO Systems in Colombia

4.1. Models Evaluated

The models implemented and evaluated in this research are the one developed by Sousa, Queluz, and Rodrigues [15] (hereinafter, also SQR model) and the Pinto I and Pinto II models [16], both for the prediction of the cumulative distribution of visibility.

4.1.1. SQR Model

Based on measurements carried out in 17 localities in Portugal over 10 years, Sousa, Queluz, and Rodrigues observed that the visibility distributions presented two clearly differentiated behaviors depending on whether they corresponded to coastal zones or inland zones. In the case of coastal zones, visibility, V [km], is given by the following [15]:

$$V_{\text{coast}} = \alpha(1 - e^{-\beta p}) \tag{2}$$

where the parameters α and β are determined from the value of $p_{(1\,\text{km})}$, which corresponds to the percentage of time for which visibility is equal to 1 km, obtained from the aver-

age number of fog days per year, N_{fd}, and the average duration of fog events, D_h (in hours), through the following:

$$p_{(1\,km)} = \frac{N_{fd}}{365.25} \cdot \frac{D_h}{24} \times 100 \quad (3)$$

In turn, the parameters α and β are calculated as follows:

$$\alpha = \frac{1}{1 - e^{-1/\tau}} \quad (\text{with } \tau = 12.6) \quad (4)$$

$$\beta = \frac{1}{\tau} \cdot \frac{1}{p_{(1\,km)}} \quad (5)$$

For inland zones, the SQR model considers an exponential-type behavior that passes through the origin [15]:

$$V_{inland} = \mu(e^{-\delta p} - 1) \quad (6)$$

with the parameters δ and μ given by the following:

$$\mu = \frac{1}{\zeta} \cdot p_{(1\,km)} \quad (\text{with } \zeta = 17.6) \quad (7)$$

$$\delta = \frac{1}{e^{(p^2_{(1\,km)}/\zeta)} - 1} \quad (8)$$

It is important to highlight that, for small values of the percentage of time, $p(\%)$, Souza et al. [15] demonstrated that visibility, for coastal and inland localities, can be calculated from the following [15]:

$$V_{sim} \approx \frac{p}{p_{(1\,km)}} \quad (9)$$

Equation (9) is useful in situations where precise information on the type of locality is not available.

Likewise, it is important to consider that the values of N_{fd} and D_h can be obtained from local measurements of visibility with a 1-min integration time, over an average annual period, with N_{fd} corresponding to the number of days in the annual period that present at least one record with visibility equal to or less than 1 km at any instant, and D_h being the number of hours associated with the aforementioned records with visibility ≤ 1 km. If such measurements are not available, estimated values reported by meteorological agencies or global databases may be used.

Finally, it should also be noted that, for the applicability of the SQR model to monthly measurement periods, as is the case of the research carried out in this work, N_{fd} will correspond to N_{fdm}, that is, the number of days in the month under study during which visibility is equal to or less than 1 km, while D_h will correspond to D_{hm}, i.e., the duration in hours of all these visibility events ≤ 1 km.

4.1.2. Pinto I and II Models

With the objective of developing a model with more global applicability than the SQR model, Pinto-Mangones et al. [16] used visibility measurements reported in the literature for Malaysia, Portugal, South Africa, and Italy, and they applied the artificial intelligence technique Particle Swarm Optimization (PSO) to fit an increasing exponential-type objective function. Thus, the first proposed model (hereinafter, also Pinto I) has the following form [16]:

$$V = 0.8839e^{0.1953p} \quad (\text{with } p \text{ in } \%) \tag{10}$$

However, Pinto-Mangones et al. [16] observed that, for visibility values below 1 km, the Pinto I model presented significant discrepancies. Therefore, they developed a second model (hereafter, also Pinto II) by intervals [16]:

$$V = \begin{cases} 0.244e^{0.2717p}, & \text{for } V_0 < 1 \text{ km} \\ 0.8839e^{0.1953p}, & \text{for } V_0 \geq 1 \text{ km} \end{cases} \tag{11}$$

where the value of V_0 is obtained from local or global visibility statistics.

4.2. Qualitative Evaluation of the Models

For the implementation of the SQR model, the values of the parameters N_{fdm} and D_{hm} were extracted from the measured visibility time series from which the cumulative distributions shown in Figure 4 were derived, resulting in the values summarized in Table 2.

Table 2. Values of N_{fdm} and D_{hm} for the localities studied.

Locality	N_{fdm}	**Measurement Events * ($V \leq 1$ km)**	D_{hm} **(Hours)**
Yopal (March 2025)	4	24	0.1
Yopal (April 2025)	N.A.	N.A.	N.A.
San Andrés (October 2024)	22	4853	3.6765
San Andrés (November 2024)	19	5073	4.45
Montería (October 2024)	8	303	0.6313
Montería (April 2025)	5	37	0.1233
Puerto Carreño (April 2025)	5	25	0.0833
Villavicencio (March 2025)	1	138	0.3091
Villavicencio (April 2025)	N.A.	N.A.	N.A.

* Refers to the number of individual 1-min records within the month during which visibility $\leq$ 1 km was recorded.

The N.A. (Not Applicable) condition in Table 2 is due to the fact that, in the measured time series for April 2025 in Yopal and Villavicencio, no visibility value $\leq$ 1 km was recorded.

Figure 5 shows the comparison between the measured cumulative visibility distributions and those estimated by the SQR model for the five localities, highlighting the following:

- In Yopal (Figure 5a), the SQR model overestimates practically all visibility values, except for very low percentages of time ($p \leq 0.03\%$), for which the measured and estimated visibility are similar. The discrepancy between the measured and estimated values becomes increasingly noticeable, from moderate to drastic, starting approximately at $p = 0.3\%$.
- In San Andrés (Figure 5b), the SQR model underestimates visibility at low and medium percentages. For $p = 0.1\%$, the measured visibility is 0.385 km (October) and 0.165 km (November), while SQR estimates it to be approximately 0.01 km in both months. For $p = 1\%$, the measured values are 0.666 km and 0.287 km, respectively, compared with 0.1 km estimated by the SQR model for both months. This trend continues, in October, throughout the entire interval of percentages of time considered, whereas in November the trend reverses from approximately $p = 4\%$ onward, from which point the visibility values are overestimated.
- In the case of Montería Figure 5c), in October, the SQR model also underestimates the visibility for most of the interval of percentages of time, except for the subinterval

between approximately $p = 0.3\%$ and $p = 2\%$, in which the measured and estimated visibility values are similar. For its part, in April, the SQR model, except for very low percentages of time ($p \leq 0.02\%$), overestimates visibility, with a trend from moderate to drastically different as the percentage of time increases, analogous to what occurs in March in Yopal.

- In Puerto Carreño (Figure 5d), the performance of the model in predicting visibility presents a behavior similar to that observed for Yopal in March and Montería in April, with a noticeable increasing overestimation for most of the percentage-of-time interval, except for low values of such percentage, in this case, approximately lower than 1%.
- In Villavicencio (Figure 5e), the SQR model tends to underestimate visibility, except approximately for the subinterval $0.2\% \leq p \leq 0.4\%$, in which the visibility values estimated by the SQR model are similar to the measured values.

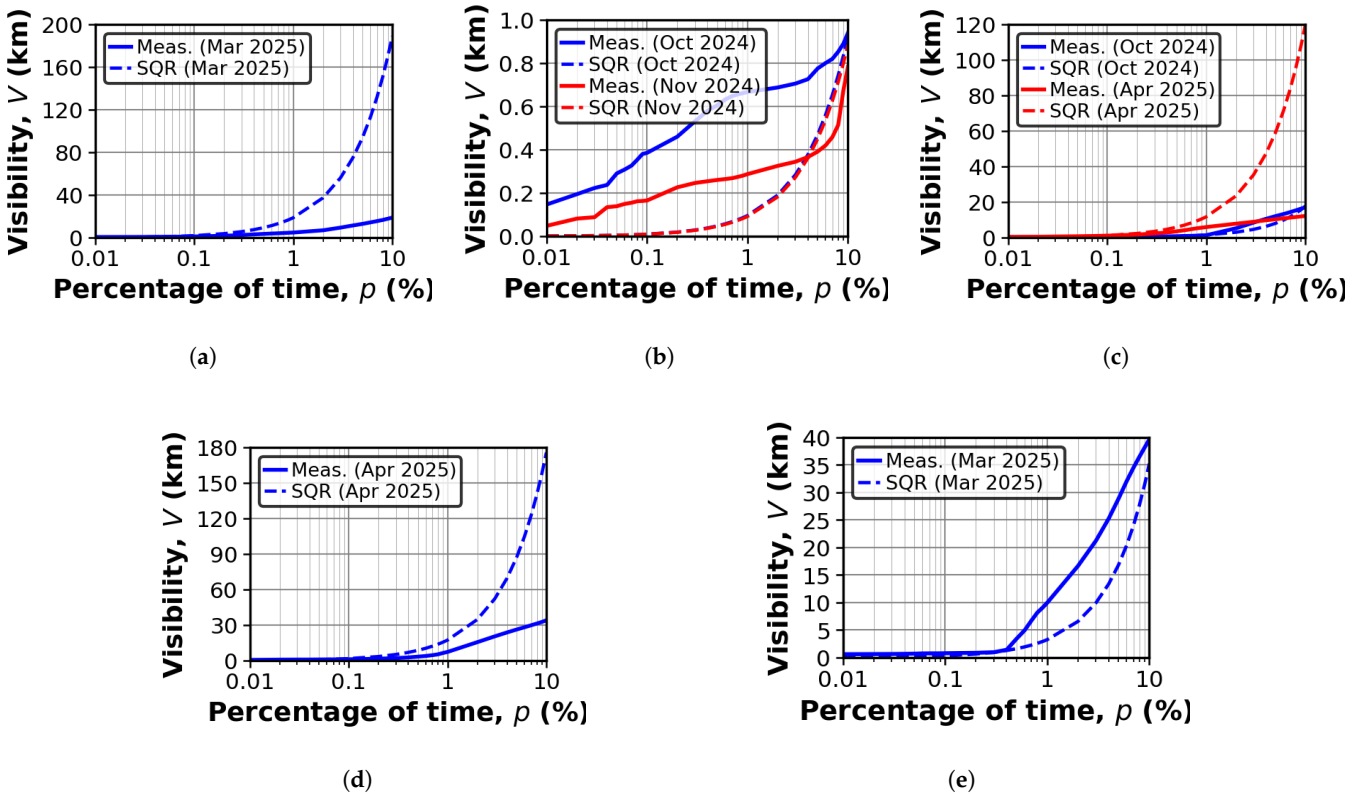


Figure 5. Cumulative visibility distributions with 1-min integration time, measured and estimated (by the SQR model) in the critical months (lowest visibility): (**a**) Yopal; (**b**) San Andrés; (**c**) Montería; (**d**) Puerto Carreño; (**e**) Villavicencio.

In turn, Figure 6 shows the cumulative distribution yielded by the Pinto I model, which is identical for all localities because it depends only on the percentage of time. It is observed that the Pinto I model underestimates visibility values for the entire interval of percentage of time and for all localities, except in the case of San Andrés, a locality for which the Pinto I model overestimates visibility throughout the entire time interval considered in this work.

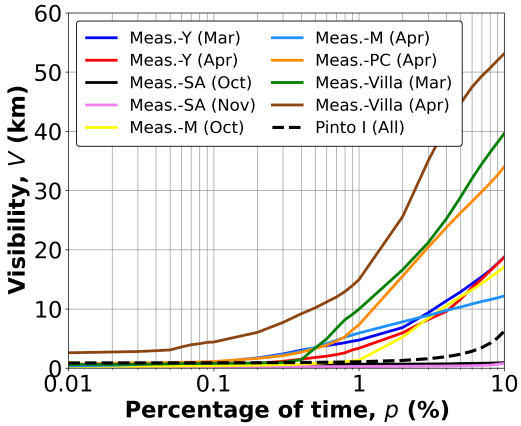


Figure 6. Measured and estimated cumulative distribution (by the Pinto I model) of visibility in Colombia, in the critical months (lowest visibility).

Regarding the visibility estimation given by the Pinto II model, the results obtained are shown in Figure 7, in which the following can be observed:

- **Yopal (Figure 7a)**: In March, the Pinto II model underestimates visibility throughout the entire interval of percentage of time, whereas in April, the estimated and measured values are similar up to $p \approx 0.04\%$, from which the model underestimates the visibility values.
- **San Andrés (Figure 7b)**: For the month of October, the Pinto II model presents two crossing points, with a slight overestimation of visibility up to $p = 0.05\%$ and a more marked one from $p = 0.04\%$ onward, underestimating visibility in the subinterval $0.05\% \leq p \leq 0.4\%$. In November, the Pinto II model overestimates visibility for the entire percentage interval considered in this research, except in the subinterval $0.2\% \leq p \leq 1\%$, in which the estimated values are similar to the measured ones. The estimated cumulative distributions are identical for both months (October and November), because the expression of the model depends only on the value of p and on the condition $V_{\text{measured}} \leq 1$ km, which is fulfilled for the entire interval of percentage of time for this locality.
- **Montería (Figure 7c)**: In October, the values estimated by the Pinto II model approximately coincide with the measurements up to $p \approx 0.09\%$ and in the subinterval $0.8\% \leq p \leq 1\%$, underestimating visibility for the remaining set of percentages of time. In April, the Pinto II model underestimates visibility throughout the entire interval of percentages, except for $p = 0.09\%$ and $p = 0.01\%$, in which the predicted and estimated values are similar. In both months, the discrepancy increases with the percentage of time.
- **Puerto Carreño (Figure 7d)**: Except for the subinterval $0.07\% \leq p \leq 0.1\%$, in which the measured and estimated values are similar, the Pinto II model underestimates visibility for the rest of the percentage-of-time interval considered in this work. Again, the discrepancy increases significantly with the increase in the percentage of time.
- **Villavicencio (Figure 7e)**: The Pinto II model underestimates visibility in both months of study, with the difference being more pronounced in April.

As can be observed in the qualitative analysis, except for the Pinto I model, whose performance in estimating visibility is clear in relation to the measured values (i.e., underestimation for all localities, except for San Andrés, in which the Pinto I model overestimates visibility), it is impossible to infer the specific performance of the SQR and Pinto II models in visibility prediction.

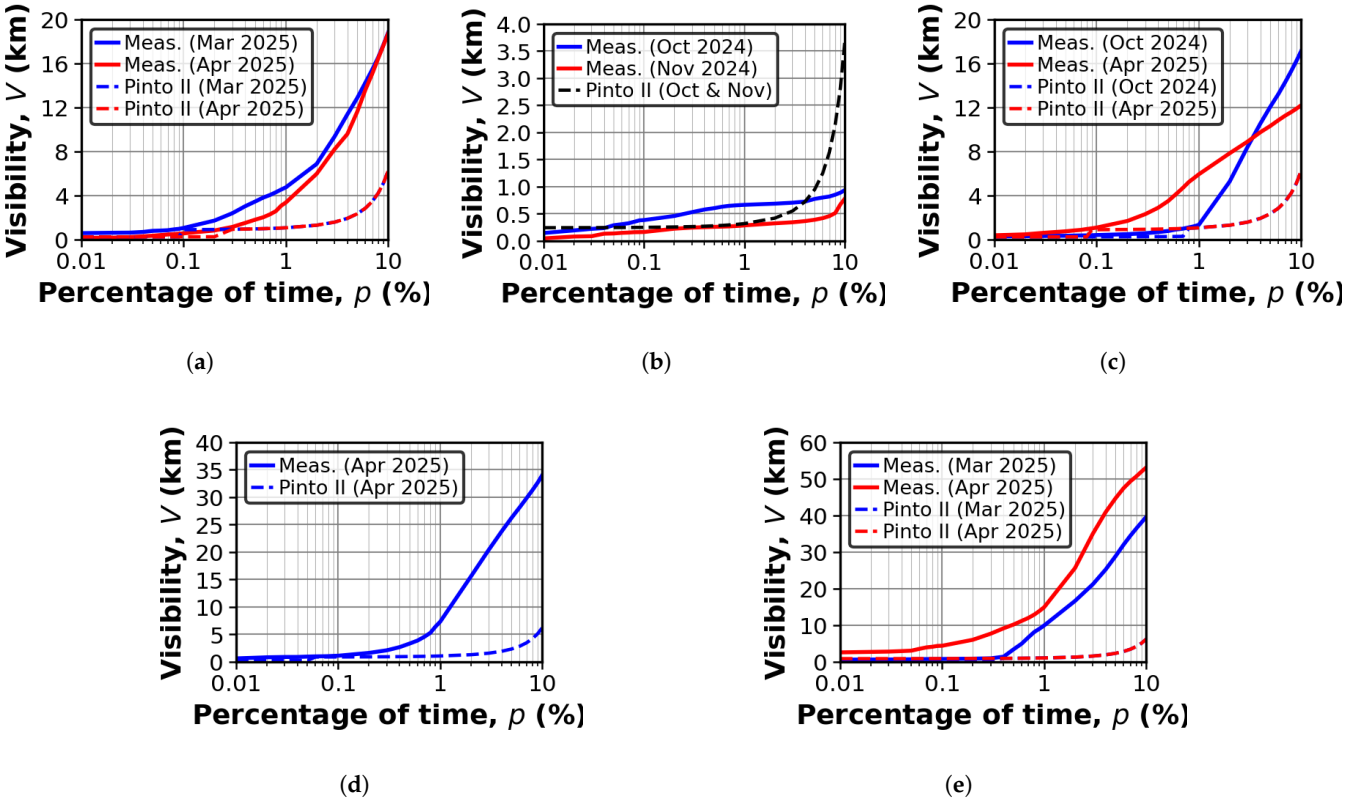


Figure 7. Cumulative visibility distributions with 1-min integration time, measured and estimated (by the Pinto II model) in the critical months (lowest visibility): (**a**) Yopal; (**b**) San Andrés; (**c**) Montería; (**d**) Puerto Carreño; (**e**) Villavicencio.

4.3. Quantitative Evaluation of the Models

In order to carry out an objective comparison of model performance, the root mean square error (RMSE) metric was used, which is widely employed in the evaluation of prediction models in telecommunications systems, defined as follows [21]:

$$\mathrm{RMSE} = \sqrt{\frac{\sum_{i=1}^{N}(V_{m,i} - V_{c,i})^2}{N}} \tag{12}$$

where $V_{m,i}$ is the measured visibility value, $V_{c,i}$ is the value estimated by the model, and N is the number of percentage-of-time points considered.

Table 3 summarizes the RMSE values obtained for each locality and evaluated model, including the global RMSE calculated over all measurements.

The global RMSE reported in Table 3 was calculated using Equation (12) applied to the complete pooled dataset of measured–estimated visibility pairs ($V_{m,i}$, $V_{c,i}$), aggregating all percentage-of-time points across all localities and months for which each model could be evaluated, rather than as an average of the per-locality RMSE values. For the SQR model, the months marked N.A. in Table 2 (Yopal, April 2025, and Villavicencio, April 2025) were excluded from this calculation, since no visibility record ≤ 1 km was provided for those months, precluding estimation of the N_{fdm} and D_{hm} parameters required by the model.

From Table 3, it follows that the SQR model performs notably well in San Andrés (RMSE < 0.4 km), where it is the best model, and acceptably in Montería (October) and Villavicencio (March), with RMSE values of 1.66 km and 6.12 km, respectively. However, it fails considerably in Yopal (March), Montería (April), and Puerto Carreño, with RMSE

values reaching 61.95 km, 194.66 km, and 49.84 km, respectively, which indicates the strong dependence of its performance on locality and seasonality.

Table 3. RMSE values (km) by locality and model.

Locality	SQR	Pinto I	Pinto II
Yopal (March 2025)	61.9511	6.2636	6.2702
Yopal (April 2025)	—	5.7949	5.7878
San Andrés (October 2024)	0.3910	1.6771	0.7305
San Andrés (November 2024)	0.1569	1.8680	0.8115
Montería (October 2024)	1.6619	5.4233	5.4176
Montería (April 2025)	194.6627	6.0079	6.0092
Puerto Carreño (April 2025)	49.8418	13.7760	13.7783
Villavicencio (March 2025)	6.1222	16.0046	16.0077
Villavicencio (April 2025)	—	24.4118	24.4118
Global	79.5129	11.4818	11.4576

Furthermore, Table 3 shows that the Pinto I and Pinto II models present practically identical behavior among themselves in all localities, with differences smaller than 0.01 km, and therefore can be considered equivalent in terms of fit. Their best relative performance occurs precisely when the SQR model fails, that is, in Yopal (March), Montería (April), and Puerto Carreño, cases in which they achieve RMSE values between 6.3 km and 13.8 km, far below the values estimated by the SQR model. Nevertheless, in localities such as San Andrés and Villavicencio (March), they are substantially outperformed by the SQR model, reaching RMSE values up to 16 times higher in the case of San Andrés.

In global terms (average over all localities and months), the Pinto I (11.48 km) and Pinto II (11.46 km) models present comparable performance and are notably superior to the SQR model (79.51 km), which suggests that, although the SQR model can be excellent in particular cases, the Pinto I and II models offer greater robustness and consistency across the total set of evaluated scenarios.

4.4. Comparison with the Approach Recommended by ITU-R P.1814-1

It is important to clarify that the SQR, Pinto I, and Pinto II models evaluated in this work belong to a different category from the specific-attenuation models (Kruse, Kim–McArthur–Korevaar) and from the approach recommended by ITU-R Recommendation P.1814-1 [11]: while the former predict the cumulative distribution of visibility, $P(V)$, from simple statistical inputs, the latter takes a known visibility distribution as input and converts it into path attenuation and link margin. Recommendation ITU-R P.1814-1 does not itself provide an analytical model to predict the visibility distribution; instead, it requires either locally measured visibility statistics or, in their absence, recommends resorting to an external database, namely, the Global Historical Climatology Network–Daily (GHCN-Daily) from the National Oceanic and Atmospheric Administration (NOAA). However, this database provides visibility records at a daily resolution, which is insufficient to capture the sub-hourly dynamics of fog formation and dissipation that are essential for the 1-min-resolution planning of FSO links, as emphasized throughout this work. Table 4 summarizes the main differences between the visibility prediction models evaluated in this study and the approach recommended by ITU-R P.1814-1 in the absence of local high-resolution data. This comparison reinforces the central motivation of this study: the reliance on coarse, non-locally validated visibility statistics—whether from empirical prediction models or from daily-resolution global databases—can introduce the same type of severe dimensioning errors illustrated in Section 5.

Table 4. Comparison of the visibility prediction models evaluated in this study with the approach recommended by ITU-R P.1814-1 in the absence of local high-resolution data.

Aspect	SQR	Pinto I	Pinto II	ITU-R P.1814-1
What it predicts	CD of visibility $V(p)$; separate equations for coastal and inland zones	CD of visibility $V(p)$; single global curve	CD of visibility $V(p)$; piecewise by $V_0 \gtrless 1$ km	Does not predict the CD of visibility; converts a known CD of visibility into path attenuation and link margin
Required statistical input	$p(1\,\text{km})$, from N_{fd} and D_h	None (function of p only)	Threshold V_0 (<1 km or $\geq$1 km)	Local visibility CCDF; in its absence, NOAA GHCN-Daily database
Temporal resolution of input	Aggregated monthly/annual statistics	Not applicable	Aggregated statistics	Recommends local high-resolution data; GHCN-Daily provides only daily resolution
Climatic calibration basis	17 Portuguese localities, temperate climate, 10 years	Malaysia, Portugal, South Africa, Italy (PSO fit)	Same as Pinto I	Global coverage via NOAA network, but no climate-specific calibration
Main limitation	Requires coastal/inland classification; no tropical validation	Predicts $V \neq 0$ at $p = 0\%$; no local-adjustment parameter	Same inconsistency at $p = 0\%$; improvement limited to $V < 1$ km	Offers no predictive alternative; in the absence of local 1-min data, recommends a resolution insufficient for accurate FSO dimensioning

5. Impact of Visibility Prediction Model Inaccuracy on the Planning and Dimensioning of FSO Systems

In order to evaluate the impact that the inaccuracy of the visibility prediction models addressed in this work would have on the planning and dimensioning of an FSO link in some of the localities considered in this research, the link margin of a hypothetical 800 m FSO link is estimated, by way of illustration, using measured and estimated visibility values for the following scenarios:

- **Scenario 1:** San Andrés, November, SQR model.
- **Scenario 2:** San Andrés, November, Pinto I model.
- **Scenario 3:** Villavicencio, April, Pinto II model.

The link margin, M (dB), is calculated as follows [22]:

$$M = P_T - A_{Tx} - 20\log\left(\frac{\sqrt{2}L\theta}{D}\right) - A_{Rx} - \gamma(V)L - S \tag{13}$$

where the following hold:

P_T = Transmitted power, in dBm.
A_{Tx} = Transmitter coupling loss, in dB.
A_{Rx} = Receiver coupling loss, in dB.
θ = Half-angle divergence, in mrad.
L = Link length, in km.
D = Receiver lens aperture diameter, in mm.
$\gamma(V)$ = Specific attenuation caused by visibility, in dB/km.
S = Receiver sensitivity, in dBm.

In this work, the specific attenuation, $\gamma(V)$, is determined using the Kim–McArthur–Korevaar model [10]. For reference, this model refines the earlier classical model pro-

posed by Kruse [9], which relates the specific attenuation to visibility through a similar power-law form:

$$\gamma(V) = \frac{3.912}{V}\left(\frac{\lambda}{550}\right)^{-q}, \quad q = 1.6 \text{ (for high visibility, } V > 50 \text{ km)} \tag{14}$$

Kim, McArthur, and Korevaar [10] later refined this expression through the piecewise definition of q given in Equation (16), adopted in this work as follows:

$$\gamma(V) = \frac{3.912}{V}\left(\frac{\lambda}{550}\right)^{-q} \tag{15}$$

where the parameter q is defined as follows [10]:

$$q = \begin{cases} 1.6 & V > 50 \text{ km} \\ 1.3 & 6 \text{ km} < V \leq 50 \text{ km} \\ 0.16V + 0.34 & 1 \text{ km} < V \leq 6 \text{ km} \\ V - 0.5 & 0.5 \text{ km} < V \leq 1 \text{ km} \\ 0 & V \leq 0.5 \text{ km} \end{cases} \tag{16}$$

where the following hold:

λ = Wavelength, in nm.
q = Factor that depends on the size distribution of the aerosol (water particles suspended in the air) that scatters the light beam.

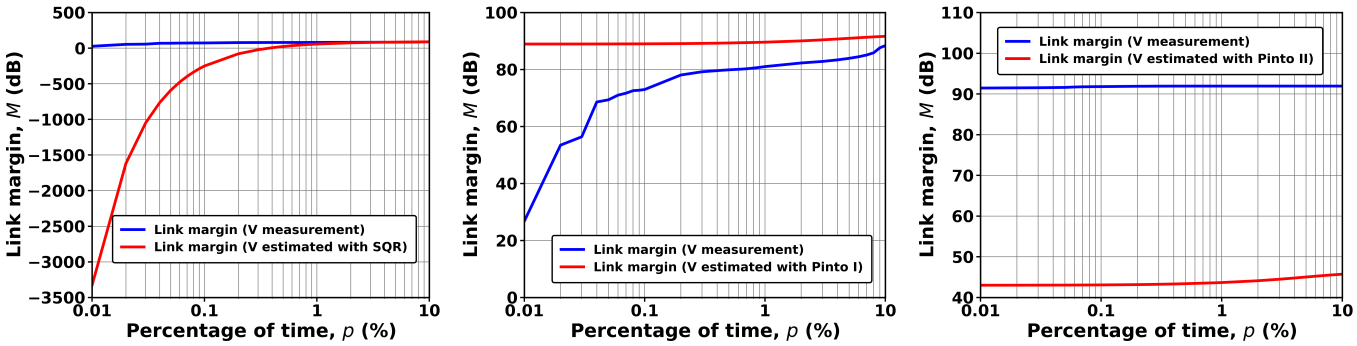
It is worth noting that this specific-attenuation model is functionally equivalent to the one recommended by the International Telecommunication Union in Recommendation ITU-R P.1814-1 [11] for the design of terrestrial FSO links, which adopts the same power-law dependence on visibility and wavelength, the same piecewise definition of the parameter q, and the same underlying 2% contrast-threshold definition of visibility (as opposed to the 5% threshold used in the WMO Meteorological Optical Range, MOR, convention). The coefficient 3.912 in Equation (15) corresponds to $-\ln(0.02)$, consistent with this 2% threshold; the ITU-R P.1814-1 Recommendation presents an equivalent coefficient of 17, which additionally incorporates the neper-to-decibel conversion factor ($4.343 \times 3.912 \approx 17$). Following common practice in the FSO literature, the visibility values obtained from the Vaisala FD70 sensor—reported under the standard WMO MOR (5%) convention—are used directly in Equation (15) without applying the formal 1.31 conversion factor between the two thresholds, consistent with how the original Kim–McArthur–Korevaar model has been applied throughout the literature. This correspondence confirms that the specific-attenuation model adopted in this work is consistent with the current ITU-R recommendation for FSO link planning.

Table 5 shows the values of the parameters involved in Equations (13), (15), and (16), taken from Singh & Mittal [22]:

Table 5. Parameter values for the link-margin calculation.

Parameter	Value
P_T	13 dBm
A_{Tx}	3 dB
A_{Rx}	3 dB
θ	1.25 mrad
D	280 mm
S	−39 dBm

Furthermore, Figure 8 shows the link-margin curves obtained for Scenarios 1, 2, and 3, contrasting the margin values obtained from the measured visibility with those obtained using the visibility models considered for each scenario.



(**a**) (**b**) (**c**)

Figure 8. Link margin: (**a**) Scenario 1 (San Andrés, November, SQR model); (**b**) Scenario 2 (San Andrés, November, Pinto I model); (**c**) Scenario 3 (Villavicencio, April, Pinto II model).

Figure 8a shows that, for San Andrés in November, the link margin calculated with the measured visibility remains positive throughout the entire range of percentages of time, reaching approximately 26 dB at $p = 0.01\%$. This indicates that the 800 m FSO link is a candidate to remain operational even during the densest fog episodes. In contrast, the margin calculated with the visibility estimated by the SQR model is catastrophically negative (for example, -3320 dB at $p = 0.01\%$), becoming positive only from $p = 0.4\%$ onward. This severe discrepancy is a direct consequence of the strong underestimation of visibility by the SQR model at low percentages, which are precisely the most relevant for link-availability dimensioning. Therefore, relying exclusively on the SQR model in this case could lead to the erroneous conclusion that the link is unfeasible or, if deployment is nevertheless pursued, to unnecessary overdimensioning.

Figure 8b shows that, for San Andrés, also in November, the link margin calculated with the visibility estimated by the Pinto I model shows minimal variation (between 89 dB and 91 dB) throughout the entire percentage-of-time interval, whereas the margin calculated with the measured visibility varies from approximately 28 dB at $p = 0.01\%$ to 88 dB at $p = 10\%$. The Pinto I model overestimates the link margin at low and medium percentages (for example, at $p = 0.01\%$, it predicts 89 dB based on the measured visibility, compared with 28 dB derived from the estimated visibility), which would lead to excessive optimism regarding link availability, thereby underestimating the real impact of dense fog. This margin overestimation is due to the fact that the Pinto I model predicts visibilities that are systematically higher than those measured in San Andrés (as observed in Figure 6), thus underestimating fog attenuation, especially at low percentages.

Finally, Figure 8c shows that, for Villavicencio in April, the link margin calculated with the measured visibility remains practically constant at around 91–92 dB throughout the entire percentage-of-time interval. In contrast, the margin calculated with the visibility estimated by the Pinto II model is significantly lower (between 43 and 47 dB), although always positive. This indicates that the Pinto II model underestimates the link margin by approximately 48 dB at low percentages, which would lead to an excessively pessimistic assessment of link feasibility, although not to the point of predicting catastrophic failure. This margin underestimation is consistent with the underestimation of visibility by the Pinto II model in Villavicencio (April), reported in Figure 7e.

6. Conclusions and Future Work

Although this study focuses specifically on the Colombian climatic context, the underlying mechanism responsible for the observed discrepancies—namely, the mismatch between the temperate/coastal climatic conditions used to calibrate the SQR, Pinto I, and Pinto II models and the convective, tropical fog dynamics observed in Colombia—is not unique to this country. Other tropical and equatorial regions with similar convective fog formation mechanisms (e.g., radiative fog over inland plains, advective coastal fog in island and littoral zones) could reasonably be expected to exhibit comparable disagreement with these models, particularly in localities analogous to San Andrés (tropical coastal) and Yopal/Puerto Carreño (transitional/inland tropical). However, this generalization cannot be confirmed without additional 1-min visibility measurements from other tropical countries, and this is identified as an important direction for future work, complementing the recommendations already outlined below.

In this work, the cumulative distributions of visibility with a one-minute integration time were presented, for the first time, for five localities in Colombia (Yopal, San Andrés, Montería, Puerto Carreño, and Villavicencio) during their respective months of lowest visibility. These distributions constitute a fundamental input for the planning and dimensioning of free-space optical (FSO) communication systems in the country, since they make it possible to estimate fog attenuation that will affect link availability.

The results obtained show that the island of San Andrés presents the most adverse conditions for the deployment of FSO systems, with visibilities below 50 m for $p = 0.01\%$ of the time during the critical month of November. This island locality, due to its tropical coastal condition, exhibits dense and persistent fogs that constitute the greatest operational challenge.

For its part, Yopal exhibits a marked seasonal behavior, with extremely critical conditions in April (visibility of 0.16 km for $p = 0.01\%$) and a convergence of the March and April curves from $p = 8\%$ onward, indicating that seasonal differences are concentrated in the lowest percentages.

In the case of Montería, a curve crossing is evident near $p = 3\%$: April is better only in the most extreme percentages of time (high), while October dominates for $3\% < p \leq 10\%$, within the range considered in this study, revealing a distribution more extended toward low values in October.

In turn, Puerto Carreño presents moderately high visibilities and a more gradual behavior than the rest of the localities, without abrupt jumps between nearby percentages.

Villavicencio, for its part, records systematically higher visibilities in April compared with March over the entire percentage range, with no crossing between the curves.

Regarding the performance of the visibility prediction models considered in this research, that is, SQR, Pinto I, and Pinto II, it is observed that the SQR model works excellently in San Andrés and acceptably in Montería (October) and Villavicencio (March), but it underperforms considerably in Yopal (March), Montería (April), and Puerto Carreño, with RMSE values reaching up to 194.66 km. Its performance is strongly dependent on locality and seasonality.

In the case of the Pinto I and Pinto II models, they exhibit practically identical behavior among themselves (differences < 0.01 km in the RMSE value). Their best relative performance occurs precisely when the SQR model fails, offering greater robustness and consistency across the total set of evaluated scenarios.

In global terms, the Pinto I and Pinto II models, with an RMSE value ≈ 11.46 km, perform better on average across the set of evaluated locations, notably outperforming the SQR model (RMSE = 79.51 km). However, the SQR model achieved the best performance under specific local conditions, such as San Andrés (RMSE < 0.4 km). This contrast

suggests that local calibration of visibility prediction models may be more relevant for accurate FSO link dimensioning than the indiscriminate selection of a single globally "best" model. It is important to consider that, even though the Pinto I and II models are easier to implement than the SQR model and also adapt, in the case of the Pinto II model, to different physical regimes of visibility (a higher slope for dense fogs and a smoother slope for better visibility conditions), they have among their disadvantages, in relation to the SQR model, the fact that they are merely empirical or phenomenological models, while the SQR model has a direct physical meaning by considering the parameters N_{fdm} and D_{hm}. In addition, the Pinto I and II models predict non-zero visibilities (0.8839 km for the Pinto I model, and 0.244 km for the Pinto II model) when $p = 0\%$, which is physically inconsistent.

This inconsistency implies that the Pinto I and Pinto II models should not be extrapolated to percentages of time below the lowest value used in their original calibration ($p \approx 0.01\%$, corresponding to the range of the datasets in [16]). Within this calibrated range, the non-zero intercept at $p = 0\%$ has negligible practical effect on link dimensioning, since FSO planning is typically concerned with small, non-zero percentages of time (e.g., $p = 0.01\%$ to 1%) rather than the limiting case $p = 0\%$. Nevertheless, this behavior should be regarded as a structural limitation of the empirical exponential form of Equations (10) and (11), rather than a physically meaningful prediction, and users of these models should restrict their application to the percentage-of-time range for which they were calibrated and validated.

The practical consequences of using visibility models that are not adjusted for the studied localities are quantified in Section 5. For example, in San Andrés, in November, the visibility value estimated with the SQR model predicts a catastrophic margin of -3320 dB for $p = 0.01\%$, compared with the 26 dB obtained using the measured visibility. The Pinto I model produces a margin overestimation of approximately 60 dB in San Andrés (for $p = 0.01\%$), also in November, whereas the Pinto II model leads to an underestimation of 48 dB in Villavicencio, in April. Therefore, it is evident that locally measured visibility data are essential to avoid both unnecessary capital expenditures and service unavailability.

Finally, as a continuation of the research carried out in this work, the following are proposed:

- Increase the visibility database, not only for the critical months (lowest visibility) but also for complete annual periods, for various localities in Colombia, in order to capture the full seasonality of visibility and reduce uncertainty in the planning and dimensioning of FSO links.
- Develop prediction models specific to Colombia, fitted directly with local measurements, models that may take the functional form of the Pinto I and II models, but incorporating adjustable parameters by locality or region, or else extending the SQR model approach through calibration of the N_{fdm} and D_{hm} parameters for tropical conditions. Additionally, it is suggested to explore artificial intelligence techniques (neural networks, support vector machines, random forests) for predicting visibility cumulative distributions from more easily accessible meteorological variables. Recent studies have shown promising results applying machine learning techniques to visibility and fog prediction in related contexts, including regression-based models for FSO path attenuation [23], ensemble learning approaches for FSO quality-of-service prediction [24], and Bayesian neural network frameworks for medium-range fog forecasting [25], supporting the feasibility of this proposed direction.
- Deploy simultaneous measurement campaigns of visibility and specific attenuation in FSO links, to evaluate, characterize, and model the attenuation–visibility relationship specifically for Colombia.

Author Contributions: Conceptualization, J.C.N.-R., D.D.Q.-C., M.E.R.-M., N.A.P.-G. and Á.D.P.-M.; Methodology, J.C.N.-R., D.D.Q.-C., N.A.P.-G. and J.M.T.-T.; Formal analysis, J.C.N.-R. and D.D.Q.-C.; Investigation, J.C.N.-R., D.D.Q.-C., M.E.R.-M. and Y.R.J.; Resources, M.E.R.-M., N.A.P.-G., Á.D.P.-M., and O.A.T.-M.; Data curation, D.D.Q.-C. and O.A.T.-M.; Writing—original draft, J.C.N.-R. and D.D.Q.-C.; Writing—review and editing, J.C.N.-R., N.A.P.-G., Á.D.P.-M., J.M.T.-T. and Y.R.J.; Funding acquisition, Á.D.P.-M. and J.M.T.-T. All authors have read and agreed to the published version of the manuscript.

Funding: This research and its open access publication were supported by Universidad del Sinú, Proyecto "Aplicaciones de la Inteligencia Artificial para la Mejora de Sistemas Teleinformáticos".

Institutional Review Board Statement: Not applicable.

Data Availability Statement: The original findings presented in this research are included in the manuscript. For any further inquiries, please contact the corresponding author. The 1-min visibility measurement data analyzed in this study were provided by the Civil Aeronautics of Colombia under a confidentiality agreement and cannot be publicly shared.

Acknowledgments: The authors would like to thank the Aeronáutica Civil de Colombia for providing the visibility time series, with a 1-min integration time, which formed the basis of this research.

Conflicts of Interest: The authors declare no conflicts of interest.

References

1. Ke, X. *Handbook of Optical Wireless Communication*; Springer: Singapore, 2024.
2. Hayle, S.T.; Cheng, M.-C.; Jiang, W.-Z.; Hsu, C.-H.; Huang, W.-T.; Lu, H.-H. A comprehensive review of FSO-UWOC hybrid systems for 5G signal transmission: Practical constraints, applications, and challenges. *Opt. Commun.* **2026**, *611*, 133174. [CrossRef]
3. Fayad, A.; Pelle, I.; Cinkler, T.; Sonkoly, B. Harnessing Free Space Optics for Efficient 6G Fronthaul Networks: Challenges and Opportunities. *Eng. Rep.* **2025**, *7*, e70051. [CrossRef]
4. Siddiky, M.N.A.; Rahman, M.E.; Uzzal, M.S.; Kabir, H.M.D. A Comprehensive Exploration of 6G Wireless Communication Technologies. *Computers* **2025**, *14*, 15. [CrossRef]
5. Sunilkumar, K.; Anand, N.; Satheesh, S.K.; Krishna Moorthy, K.; Ilavazhagan, G. Radiative effects of atmospheric aerosols on the average channel capacity of free-space optical communication systems. *Appl. Opt.* **2021**, *60*, 9957–9965. [CrossRef] [PubMed]
6. Stassinakis, A.N.; Chatzikontis, E.V.; Drexler, K.R.; Tsigopoulos, A.D.; Mkrttchian, G.M.; Nistazakis, H.E. Semi-Empirical Estimation of Aerosol Particle Influence at the Performance of Terrestrial FSO Links over the Sea. *Computation* **2026**, *14*, 39. [CrossRef]
7. Alhartomi, M.A.; Abdullah, M.F.L.; Mabrouk, W.A.B.; Gismalla, M.S.M.; Alzahmi, A.; Alzahrani, S.; Altimania, M.R.; Alsawat, M.S. Performance Analysis of Curved Track G2T-FSO (Ground-to-Train Free Space Optical) Model under Various Weather Conditions. *CMES-Comput. Model. Eng. Sci.* **2024**, *141*, 3. [CrossRef]
8. World Meteorological Organization. *Guide to Meteorological Instruments and Methods of Observation. (WMO-No. 8), Volume I*; World Meteorological Organization: Geneva, Switzerland, 2024. Available online: https://library.wmo.int/records/item/68695-guide-to-instruments-and-methods-of-observation (accessed on 15 March 2026).
9. Kruse, P.W.; McGlauchlin, L.D.; McQuistan, R.B. *Elements of Infrared Technology: Generation, Transmission and Detection*; Wiley: New York, NY, USA, 1962.
10. Kim, I.I.; McArthur, B.; Korevaar, E.J. Comparison of laser beam propagation at 785 nm and 1550 nm in fog and haze for optical wireless communications. In *Proceedings of the SPIE (Society of Photo-Optical Instrumentation Engineers), Optical Wireless Communications III, Boston, MA, USA, 5–8 November 2000*; SPIE: Bellingham, WA, USA, 2001; Volume 4214, pp. 26–37. [CrossRef]
11. International Telecommunication Union. *ITU-R Recommendation P.1814-1: Prediction Methods Required for the Design of Terrestrial Free-Space Optical Links*; International Telecommunication Union (ITU): Geneva, Switzerland, 2025. Available online: https://www.itu.int/rec/R-REC-P.1814/en (accessed on 6 February 2026).
12. Kvicera, V.; Grabner, M.; Vasicek, J. Assessing availability performances of free space optical links from airport visibility data. In *Proceedings of the 7th International Symposium on Communication Systems, Networks & Digital Signal Processing (CSNDSP 2010), Newcastle Upon Tyne, UK, 21–23 July 2010*; IEEE: Piscataway, NJ, USA, 2010; pp. 562–565. [CrossRef]
13. International Telecommunication Union. *ITU-R Recommendation P.581-3: The Concept of "Worst Month"*; International Telecommunication Union (ITU): Geneva, Switzerland, 2022. Available online: https://www.itu.int/rec/R-REC-P.581/en (accessed on 17 April 2026).

14. International Telecommunication Union. *ITU-R Recommendation P.837-8: Characteristics of Precipitation for Propagation Modelling*; International Telecommunication Union (ITU): Geneva, Switzerland, 2025. Available online: https://www.itu.int/rec/R-REC-P.837/en (accessed on 30 April 2026).
15. Sousa, I.; Queluz, M.P.; Rodrigues, A. An Efficient Visibility Prediction Framework for Free-Space Optical Systems. *CMES-Wirel. Pers. Commun.* **2017**, *96*, 3483–3498. [CrossRef]
16. Pinto-Mangones, A.D.; Camacho-Abreu, A.G.; Pérez-García, N.A.; Rivera-Julio, Y.E.; Torres-Tovio, J.M.; Ibarra-Hernández, F.A.; Castaño-Rivera, S.O.; Guevara-Salgado, P.R. Nuevo Modelo para la Predicción de la Visibilidad, para Uso en la Planificación y Dimensionamiento de Sistemas de Comunicaciones Ópticas en el Espacio Libre. *Rev. Ibérica Sist. Tecnol. Informação* **2023**, *E60*, 682–694.
17. Pinto-Mangones, A.D.; Rivera-Julio, Y.E.; Pérez-García, N.A.; Torres-Tovio, J.M.; Marquez-Guardia, N.E.; Garcia-Hoyos, R.; Ramirez-Marquez, D.C.; Ibarra-Hernández, F.A. New Indoor Propagation-Loss Prediction Model for WLANs Using the GRG Technique. In *Proceedings of the 2025 IEEE Colombian Caribbean Conference (C3), Santa Marta, Colombia, 17–20 September 2025*; IEEE: Piscataway, NJ, USA, 2025; pp. 1–6. [CrossRef]
18. Vaisala. *Forward Scatter Sensor FD70*; Vaisala: Vantaa, Finland, 2024. Available online: https://docs.vaisala.com/v/u/B211744EN-H/en-US (accessed on 27 March 2026).
19. Ferlic, N.A. Forward Scattering Meter for Visibility Measurements. Master's Thesis, University of Maryland, Washington, DC, USA, 2019.
20. Oh, Y.J.; Suh, M.S. Development of Quality Control Method for Visibility Data Based on the Characteristics of Visibility Data. *Korean J. Remote Sens.* **2020**, *36*, 707–723. [CrossRef]
21. Pinto-Mangones, A.D.; Pérez-García, N.A.; Castillo-Rondón, J.J.; Castillo-Sánchez, J.A.; Torres-Tovio, J.M.; Ibarra-Hernández, F.A.; Rivera-Julio, Y.E.; Yepes-Escobar, J.A. Adjustment of the ITU-R Model for the Rainfall Attenuation Prediction in Satellite Links, by Applying Industry X.0 Base Technology. In *Proceedings of the 17th IEEE Colombian Conference on Communications and Computing (COLCOM 2024), Barranquilla, Colombia, 21–23 August 2024*; IEEE: Piscataway, NJ, USA, 2024; pp. 1–6. [CrossRef]
22. Singh, H.; Mittal, N. Link budget analysis of free space optical communication link for atmospheric conditions of India. *Mater. Today Proc.* **2022**, *48*, 1064–1069. [CrossRef]
23. Aborisade, O.B.; Ojo, J.S.; Owolawi, P.; Adedayo, K.D. Machine Learning-Based Prediction of Path Attenuation Coefficient for Terrestrial FSO Link: Northern Cape, South Africa. In *Proceedings of the 8th URSI-NG Annual Conference (URSI-NG 2024), Akure, Nigeria, 20–22 March 2024*; Atlantis Press: Dordrecht, The Netherlands, 2025; pp. 199–212. [CrossRef] [PubMed]
24. Adebusola, S.O.; Owolawi, P.A.; Ojo, J.S.; Maswikaneng, P.S. Optimized quality of service prediction in FSO links over South Africa using ensemble learning. *Opt. Commun.* **2025**, *579*, 131509. [CrossRef]
25. Deshpande, P.; Bhattacharya, A.; Tripathi, S. FogCast: Probabilistic medium-range fog forecasting using global machine-learning weather prediction model. *Q. J. R. Meteorol. Soc.* **2026**, *152*, e70150. [CrossRef]

Disclaimer/Publisher's Note: The statements, opinions and data contained in all publications are solely those of the individual author(s) and contributor(s) and not of MDPI and/or the editor(s). MDPI and/or the editor(s) disclaim responsibility for any injury to people or property resulting from any ideas, methods, instructions or products referred to in the content.